Earth and Planetary Science Letters 610 (2023) 118098

Contents lists available at ScienceDirect

Earth and Planetary Science Letters

journal homepage: www.elsevier.com/locate/epsl

The India-Asia collision results from two possible pre-collisional crustal configurations of northern Greater India

Yipeng Li *, Delores M. Robinson

Department of Geological Sciences, the University of Alabama, United States of America

ARTICLE INFO

Article history:
Received 21 October 2022
Received in revised form 6 February 2023
Accepted 28 February 2023
Available online xxxx
Editor: A. Webb

Keywords:
continental collision
Himalaya
mass balance analysis
Greater India

ABSTRACT

Interpretations of pre-collisional configurations of Greater India are highly controversial and predict distinct processes during the India-Asia collision. To better determine the possible pre-collisional configuration(s) of Greater India, we conduct a mass-balance analysis combined with previously published geologic, paleomagnetic, and geodynamic evidence. The mass-balance analysis determines the magnitude of northern Greater India (NGI) width needed to provide sufficient crustal accretion to form the Tethyan-Greater Himalaya orogenic wedge in Cenozoic time. Applying endmember crustal thicknesses of 10–40 km to a mass-balance equation yields a broad range of plausible pre-collisional NGI widths of ~3016±1000 km and ~956±283 km, respectively, which we further assess considering contrasting models/evidence. The integrated evidence requires a thin NGI continental crust to form 1) continuous Tethyan-Greater Himalayan crustal thickening, 2) a narrow foredeep width of Himalayan foreland basin, 3) continuous Gangdese arc magmatism with oceanic-subduction-style mantle wedge, and 4) low-magnitude exhumation in the North Himalaya and Gangdese arc-forearc from ~60-30 Ma. Adding the structurally restored ~740 km wide southern Greater India, the synthesized analyses yield two possible configurations: 1) an ~1350±440 km wide and ~23-30 km thick NGI indicating an ~2080±450 km wide Greater India with ~500-1000 km wide oceanic basin systems in both Asia and NGI; and 2) a ≥1815±630 km wide and ~10-23 km thick Zealandia-type NGI indicating a ≥2550±640 km wide pre-collisional Greater India without or with limited ~500-1000 km Xigaze back-arc oceanic basin. The former is conditionally consistent with the integrated evidence by assuming no Cenozoic oceanic subduction initiation within NGI and predicts multi-stage collision since ~60 Ma. The latter is consistent with the integrated evidence and predicts an approximate-single-stage collision at ~60 Ma. Both configurations predict significant post-collisional NGI crustal shortening that may have been accommodated by the Eocene-Oligocene Greater Himalayan structural discontinuities.

Published by Elsevier B.V.

1. Introduction

The Cenozoic India-Asia continental collision is used to analogize global continental tectonic processes. The distribution, extent, magnitude, and timing of intracontinental deformation and surface uplift, and related global effects on climate and mantle geochemistry during the India-Asia collision are primarily controlled by the timing and duration of the collision and the magnitudes of post-collisional convergence (e.g., Hodges, 2000; Yin and Harrison, 2000; Ingalls et al., 2016; Ding et al., 2017, 2022). However, conflicting geologic and paleomagnetic studies yield highly variable interpretations of these controlling parameters. Geologic records generally indicate initial timing of ~60±5 Ma for the India-Asia collision with <2000 km post-collisional upper crustal shortening in Asia and India (Yin and Harrison, 2000; Hodges, 2000; Van Hinsbergen et al., 2011a; Cai et al., 2011; DeCelles et al., 2014; Robinson and Martin, 2014; Hu et al., 2015; Ding et al., 2005, 2016, 2022). In contrast, paleomagnetic studies document a large paleolatitude gap of ~5600-3200 km between Asia and India at ~65-55 Ma, which significantly exceeds the <2000 km of intracontinental shortening leading to a shortening deficit, primarily during ~60-30 Ma (e.g., Van Hinsbergen et al., 2012). To solve the shortening deficit problem, we need to know the pre-collisional configurations of both plates. Two-stage collisional models have been proposed by creating a large-scale oceanic basin in the Indian or Asian plates prior to the collision to compensate for the shortening deficit (Figs. 1a-b). However, the existence and location of the proposed oceanic basins are highly debated due to the lack of surface geological records (DeCelles et al., 2014; Kapp and DeCelles, 2019).

* Corresponding author.
E-mail address: yli268@ua.edu (Y. Li).

https://doi.org/10.1016/j.epsl.2023.118098
0012-821X/Published by Elsevier B.V.

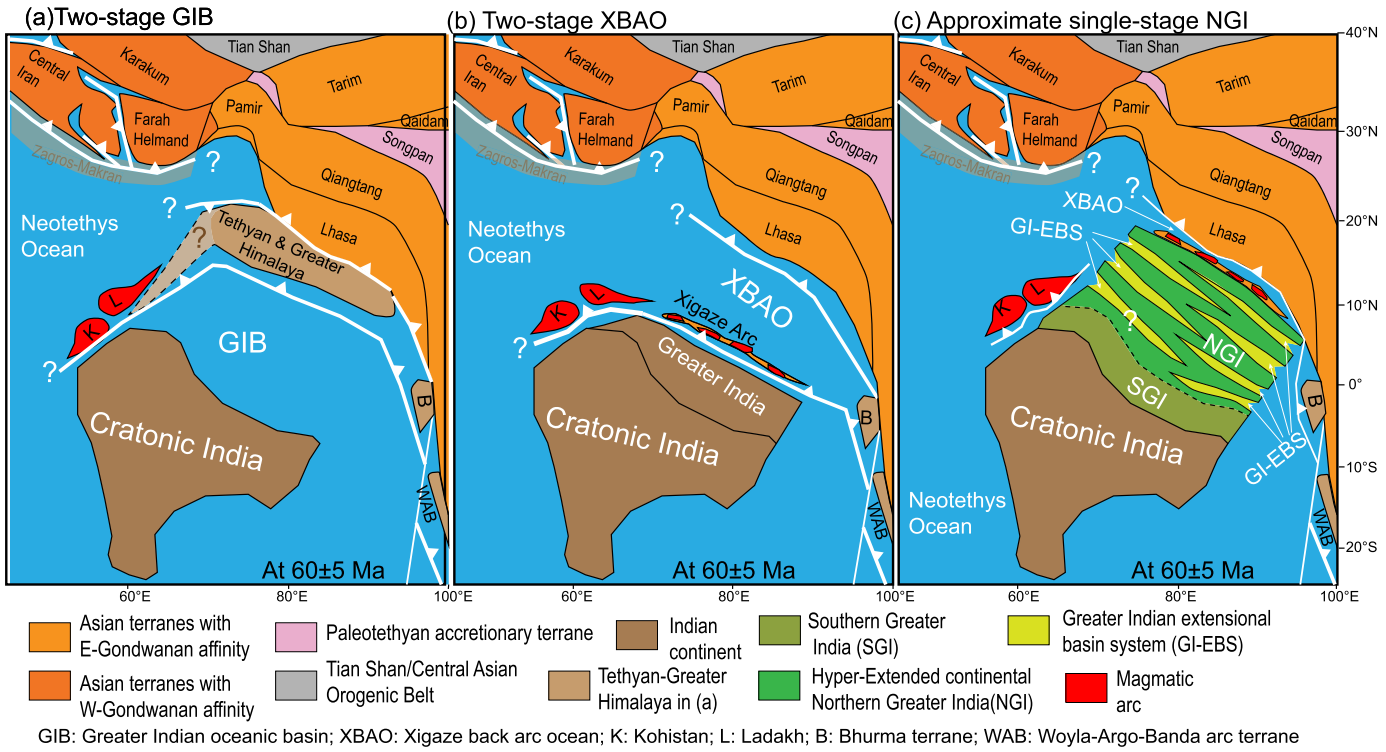

Fig. 1. Proposed India-Asia collision models. a) Two-stage hypothesis of Greater Indian oceanic basin collision model (GIB) (Van Hinsbergen et al., 2012). b) Two-stage hypothesis of Xigaze-Trans-Tethyan back-arc ocean (Cai et al., 2011; Kapp and DeCelles, 2019). c) Approximate one-stage hypothesis of hyper-extended continental NGI in this study.

Significant debates and uncertainties regarding the pre-collisional configurations of both plates largely result from a key difficulty: Greater India has been completely consumed in Cenozoic time, which results in the pre-collisional configuration not being fully constrained by the current geologic, paleomagnetic, and geodynamic data. However, there is consensus that the Tethyan-Greater Himalaya (TGH) requires sufficient middle-upper crust material sourced from the northern portion of pre-collisional Greater India, which we refer to northern Greater India (NGI), to contribute to the post-collisional crustal accretion from ~60-30 Ma (DeCelles et al., 2002; Kapp and DeCelles, 2019). This permits a middle-upper crustal mass-balance relationship between the pre-collisional NGI configuration (Fig. 1a–c, Fig. 3) and post-collisional TGH accretion coeval with the shortening deficit. The mass-balance relationship combined with the integrated results from previous geologic, paleomagnetic, and geodynamic studies provide an alternative opportunity to constrain the NGI configuration. In this study, we first conduct a quantitative mass-balance analysis between the N-S NGI width and Himalayan crustal accretion to determine the mass-balance-allowed NGI configurations from thick-and-narrow to thin-and-wide. Further, we use paleomagnetic evidence to determine whether oceanic basins are needed on either or both plates in these configurations and, if needed, what the permissible oceanic basin sizes are. Finally, we appraise what NGI configurations best fit the geologic-geodynamic evidence and determine whether the integrated results indicate other possible tectonic models.

2. Geological background

The Himalayan orogenic belt is located along the southern margin of the Tibetan Plateau (Fig. 2). In the Himalaya, the tectonostratigraphic units are from south to north the Subhimalaya, Lesser Himalaya, Greater Himalaya, and Tethyan Himalaya, and are bracketed by the south-directed Main Frontal thrust in the south and the north-directed Great Counter thrust in the north (Fig. 2) (i.e., Hodges, 2000; Yin, 2006). The south-directed Main Boundary and Main Central thrusts and the north-directed Southern Tibetan detachment system structurally juxtapose these tectonostratigraphic units (Fig. 2).

Tethyan Himalayan rocks contain meta-sedimentary and sedimentary sequences with ages from late Neoproterozoic to Eocene time (Hodges, 2000), and are the cover sequence to Greater Himalayan rocks (Martin, 2017). Greater Himalayan rocks are metamorphosed from a Neoproterozoic to early Cambrian protolith. Rocks in both domains have evolved continental crustal ε(Nd) values of -15 to -20 (Robinson et al., 2001; Murphy, 2007). Greater Himalayan rocks document upper amphibolite to granulite facies peak metamorphism interpreted to occur at ~35-25 Ma followed by regional exhumation and leucogranitic partial melting from ~25-15 Ma (e.g., Kohn, 2014; Wu et al., 2020). Petrochronology yields metamorphic ages from ~55-30 Ma in the TGH metamorphic rocks, which indicates an early-stage of crustal thickening (e.g., Smit et al., 2014; Lihter et al., 2022). Recently recognized Himalayan ductile thrust discontinuities accommodated N-S shortening from ~40-25 Ma coeval with crustal thickening (e.g., Carosi et al., 2018). The TGH and Lesser-Subhimalayan rocks are the material from distal and proximal Greater India, respectively (DeCelles et al., 2002; Myrow et al., 2003). We refer to the Lesser-Subhimalayan rocks as southern Greater India (SGI), and to the TGH as northern Greater India (NGI) (Fig. 2). Total Cenozoic shortening across Greater India, now present in the Himalaya, is <~1000 km (Robinson and Martin, 2014 and references therein), with the magnitude of crustal shortening from 60-30 Ma poorly constrained (Robinson and Metcalf, 2020).

In this study, Asia refers to the Tibetan Plateau terranes (Fig. 2) (cf., Yin and Harrison, 2000). In Asia, minimum upper crustal shortening from Mongolia to the Great Counter thrust since ~60 Ma is ~700 km (Table S1) (Yin and Harrison, 2000; Van Hinsbergen et al., 2011a). Syn-collisional paleo-latitudes of southern Lhasa

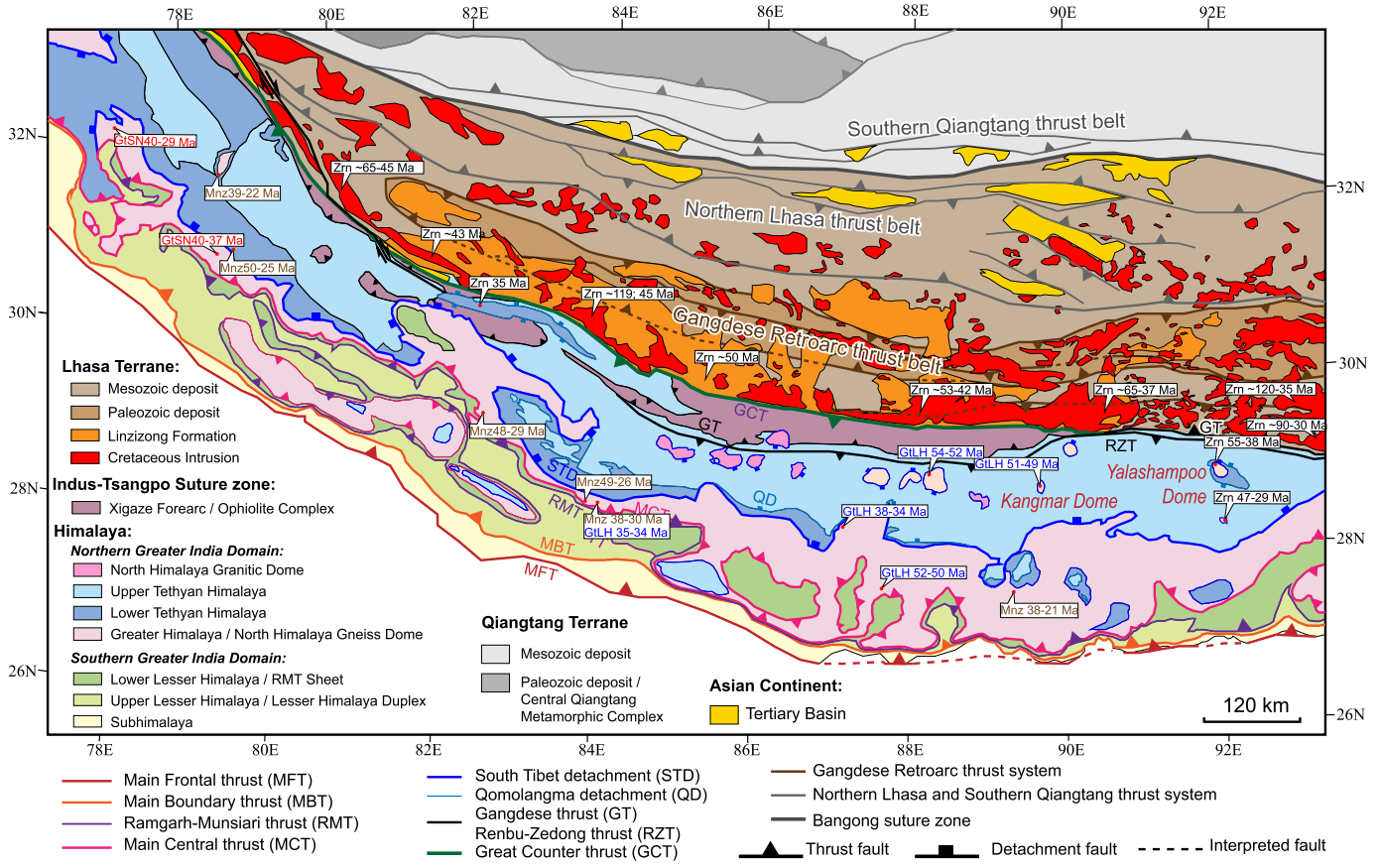

Fig. 2. Regional geologic map of the Himalaya and Tibetan Plateau. Modified primarily from Pan et al. (2004) and Robinson et al. (2021). GtLH: garnet Lu-Hf ages; GtSN: garnet Sm-Nd ages; Mnz: monazite U-Th-Pb ages; Zrn: zircon U-Pb ages. References in Table S5 for ages in the Himalaya, Table S6 for the ages in the Gangdese arc, and Table S8 for structures in Tibetan Plateau.

ranges from ~10-30°N, indicating available magnitudes of ~0-2000 km of Cenozoic Asian crustal shortening (Yi et al., 2021 and references therein). Here we adopt a compromised/conservative magnitude of ~1000 km for Asian intracontinental convergence since ~60 Ma. In the southernmost Lhasa terrane, the Gangdese arc has long-lasting calc-alkaline magmatism from ~100-30 Ma with relatively juvenile ε(Nd) values from -5 to +5 (i.e., Jiang et al., 2014). Along the southern Gangdese arc system, the Xigaze arc may represent an arc terrane rifted off the southern Asian margin from ~90-70 Ma and tectonically correspond to the Kohistan-Ladakh-Spong intraoceanic arc system, which may significantly broaden the southern Asian margin to the south for thousands of kilometers in Paleocene time (Fig. 1b) (Kapp and DeCelles, 2019 and references therein). In the west, <200 km of Cenozoic N-S shortening in the Pamir-Karakoram terranes and the lack of Lhasa terrane equivalent result in a significant northward deflection and embayment of the southern Asian margin (Li et al., 2020) (Figs. 1a-c). The paleolatitude of Ladakh and timing of the India-Kohistan-Ladakh collision at ~56-55 Ma result in an oceanic basin, the Kshiroda or Shyok basin, between the Kohistan-Ladakh and Pamir-Karakoram (Fig. 1a-c) (Ding et al., 2016; Martin et al., 2020).

3. Mass-balance analysis

3.1. Setup of the mass-balance equation

Crustal mass-balance analysis has been widely used in understanding mass transfer from Greater India to Tibet-Himalaya during the India-Asia collision (i.e., Ingalls et al., 2016). Based on end-member subduction-accretion models (Cowgill et al., 2016), the upper portion of the downgoing lithosphere will be accreted into the orogenic wedge with the lower portion subducted (Fig. 3). TGH crustal thickening and regional metamorphism, which began at ~60-55 Ma and lasted until 30-25 Ma, indicate that the TGH accommodates most of the crustal accretion from NGI convergence during ~60-30 Ma. Moreover, we consider: 1) insignificant mass transfer from NGI to Tibet at depth from ~60-30 Ma due to juvenile ε(Nd) values in Cenozoic magmatic rocks of the Lhasa-Gangdese arc until ~25-20 Ma (e.g., Jiang et al., 2014); and 2) insignificant mass transfer from Lhasa-Gangdese arc to the Himalaya due to evolved ε(Nd) values of Cenozoic igneous-metamorphic rocks in the TGH without juvenile signatures (i.e., Aikman et al., 2012). Therefore, a 3D mass-balance relationship can be established directly from NGI convergence to TGH accretion, with the subducted NGI lithosphere and Tibetan crust not considered:

$$\iint_{A} (\rho_{NGI} \cdot ACT_{NGI}) dA = \iint_{A} \left(\rho_{BTGH} \cdot T_{TGH}^{sl} + \rho_{UTGH} \cdot ER \cdot t \right) dA \quad (1)$$

ρ_{NGI}, ρ_{BTGH}, and ρ_{UTGH} represent the mid-upper NGI crustal density and bulk- and upper-crustal densities of the TGH, respectively. ACT_{NGI} represents the average accreted crustal thickness of the pre-collisional NGI that scraped-off during Cenozoic subduction-accretion. T_{TGH}^{sl} is the TGH crustal thickness at a specific locality at 30 Ma; A is land area in a planar coordinate system; ER is long-term average erosion rate; t is the duration of crustal accretion.

Minor post-collisional Cenozoic crustal shortening in the Lhasa terrane (Kapp and DeCelles, 2019 and references therein) indicates a relatively rigid Gangdese-Lhasa buttress for TGH crustal accretion

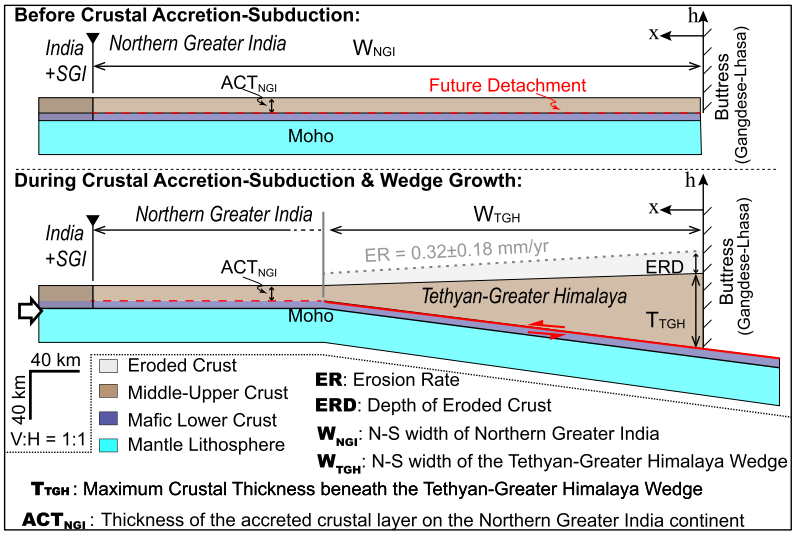

Fig. 3. Graphic illustration of mass-balance setup; the values of the parameters are provided in Tables 1 and S1.

(Fig. 3). We further consider an along-strike invariable TGH wedge shape and a NGI with a uniform N-S size, E-W width, and average thicknesses of the accreted crustal layers (Fig. 3). Equation (1) can be written as:

$$L_{NGI}\int_0^{W_{NGI}}(\rho_{NGI}\cdot ACT_{NGI})\,dx = L_{TGH}\int_0^{W_{TGH}}\left[\rho_{BTGH}\left(T_{TGH}-\frac{T_{TGH}-ACT_{NGI}}{W_{TGH}}\cdot x\right)+\rho_{UTGH}\cdot ER\cdot t\right]dx \quad (2)$$

Integrating both sides:

$$L_{NGI}\cdot\rho_{NGI}\cdot ACT_{NGI}\cdot W_{NGI} = L_{TGH}\cdot W_{TGH}\cdot\left[\rho_{BTGH}\cdot\frac{1}{2}(ACT_{NGI}+T_{TGH})+\rho_{UTGH}\cdot ER\cdot t\right] \quad (3)$$

W_{NGI} and W_{TGH} represent the strike-normal horizontal widths of pre-collisional NGI and the TGH at 30 Ma, respectively; T_{TGH} is the maximum thickness of the TGH wedge at ~30 Ma; L_{NGI} and L_{TGH} represent the E-W length of NGI and TGH, respectively. x is the horizontal component.

As the E-W length does not change from the Main Frontal thrust to the Indus-Yarlu suture in map-view, and no evidence exists to indicate that the Himalayan orogen experienced significant E-W extension or contraction in Cenozoic time, we have:

$$L_{NGI} = L_{TGH}$$

Using this relationship, we simplify Equation (3) in 2D and divide it by ρ_{NGI} and ACT_{NGI} to yield the primary mass-balance equation:

$$W_{NGI} = \frac{W_{TGH}}{ACT_{NGI}}\left[\frac{\rho_{BTGH}}{\rho_{NGI}}\cdot\frac{1}{2}(ACT_{NGI}+T_{TGH})+\frac{\rho_{UTGH}}{\rho_{NGI}}\cdot ER\cdot t\right] \quad (4)$$

Therefore, we establish a quantitative relationship between the pre-collisional NGI configuration characterized by W_{NGI} and ACT_{NGI} and the status of TGH characterized by the width-thickness, erosion rate, and duration of accretion.

3.2. Parameter analysis

As the original NGI lithosphere has been completely consumed, the W_{NGI} and ACT_{NGI} are unknown variables that need to be determined by combining mass-balance with other evidence. The TGH-related variables can be determined by regional geology. T_{TGH} is ~70 km thick based on peak metamorphic pressure of 20-21 kbar of the Ama Drime granulite at 30 Ma (Table S1). W_{TGH} at ~30 Ma is ~410 km wide calculated by measuring present-day N-S width of the TGH integrated with the Oligo-Miocene TGH internal shortening (Table S1) (Murphy and Yin, 2003; Webb, 2013). An average erosion rate during ~60-30 Ma cannot be directly determined from the Himalaya. Therefore, we integrate the long-term average erosion rates of 0.1-0.9 mm/yr from collisional fold-thrust belts with ~1000-2000 m elevation at middle-to-low latitude, including the Zagros, Carpathian, Southern Andes, and Lesser Himalaya (Table S1). To determine the best value, we apply the non-parametric Kernel density estimation to the erosion rate dataset, which consistently yields the highest probability-density value of 0.32 mm/yr using different probability-density functions, consistent with the mean, median, and mode of 0.39, 0.33, and 0.3 mm/yr, respectively (Table S2). The duration t is 30 myr as determined from the early-stage post-collisional convergence from ~60-30 Ma, corresponding to the shortening deficit and the TGH prograde-to-peak metamorphism from ~60-55 to ~30-25 Ma. All the parameters are listed in Table 1.

3.3. Uncertainty analysis

The uncertainties of the parameters significantly affect the validity of mass-balance analysis. Combined uncertainty of T_{TGH} is estimated as ±10 km or ±3 kbar considering thermodynamic and geologic-analytical sampling uncertainties (Table S1). For W_{TGH}, 9 measurements yield an average deviation of ±25 km, which we further enlarge 2-times to ±50 km to cover other unknown error sources (Table S1). For erosion rate, 17 data points yield an average deviation of ±0.18 mm/yr (Table S2). Moreover, we also assign a ±10 Myr to t for analysis; however, the densities and 30 Myr of accretion are preconditions, which we interpret to not contribute to the uncertainties of the final result.

For pre-collisional NGI configurations, we are most interested in W_{NGI}, with ACT_{NGI} varying from the surface to Moho depth. The parameters are independent, which indicate the items including second-order mixed derivatives can be ignored. Therefore, the er-

Table 1
Parameters and variables used in Mass-balance calculation.

Parameter	Symbol	Value	Uncertainty	Unit	Note
N-S width of TGH	W_{TGH}	410	±50	km	
Maximum thickness of TGH	T_{TGH}	70	±10	km	
Long-term average erosion rate	ER	0.32	±0.18	mm/yr	Using KDE
Duration of TGH accretion	t	30	-	Myr	Early-stage metamorphism from ~60-55 Ma to 30-25 Ma
Density of TGH upper crust	ρ_{UTGH}	2750	-	kg/m^3	
Density of TGH bulk crust	ρ_{BTGH}	2800	-	kg/m^3	
Density of NGI mid-upper crust	ρ_{NGI}	2650	-	kg/m^3	
Estimated Variable					
Thickness of accreted NGI crustal layer	ACT_{NGI}	5-40	-	km	Equal to NGI mid-upper crustal thickness
Middle-upper NGI crustal thickness	MUT_{NGI}	7-27	-	km	
Bulk NGI crustal thickness	T_{NGI}	10-40	-	km	
Calculated Variable					
N-S width of Northern Greater India	W_{NGI}	698-3017	±197-999	km	With NGI crustal thickness from ~10-40 km
N-S width of Southern Greater India	W_{SGI}	736	±99	km	Calculated from balance cross-section
N-S width of pre-collisional Greater India	W_{GI}	1093-3301	±239-922	km	With NGI crustal thickness from ~10-40 km

Densities from Christensen and Mooney (1995)

ror propagation from the parameter uncertainties to ΔW_{NGI} can be written as (Zou, 2014):

$$\begin{aligned}\Delta W_{NGI} &= \frac{\partial W_{NGI}}{\partial W_{TGH}}\Delta W_{TGH} + \frac{\partial W_{NGI}}{\partial T_{TGH}}\Delta T_{TGH} + \frac{\partial W_{NGI}}{\partial ER}\Delta ER \\ &\quad + \frac{\partial W_{NGI}}{\partial t}\Delta t \\ &= \frac{\left[\frac{\rho_{BTGH}}{\rho_{NGI}}\cdot\frac{1}{2}\left(ACT_{NGI}+T_{TGH}\right)+\frac{\rho_{UTGH}}{\rho_{NGI}}\cdot ER\cdot t\right]}{ACT_{NGI}}\Delta W_{TGH} \\ &\quad + \left(\frac{1}{2}\frac{\rho_{BTGH}}{\rho_{NGI}}\cdot\frac{W_{TGH}}{ACT_{NGI}}\right)\Delta T_{TGH} \\ &\quad + \left(\frac{\rho_{UTGH}}{\rho_{NGI}}\cdot\frac{W_{TGH}}{ACT_{NGI}}\cdot t\right)\Delta ER \\ &\quad + \left(\frac{\rho_{UTGH}}{\rho_{NGI}}\cdot\frac{W_{TGH}}{ACT_{NGI}}\cdot ER\right)\Delta t\end{aligned} \quad (5)$$

Figs. 4a-f and Table S3 show the total uncertainty of W_{NGI} and partial contributions from each parameter uncertainty using equation (5) (abbreviations in Table 1), which consistently shift W_{NGI} in the positive direction. Both total and partial ΔW_{NGI} decrease with ACT_{NGI} increasing and significantly increase at ACT_{NGI} <10 km (Figs. 4a-f). Using the parameter values in Table 1 and the parameter uncertainties including ΔW_{TGH} of ±50 km, ΔT_{TGH} of ±10 km, ΔER of ±0.18 mm/yr, and Δt ±10 of Ma, error propagation equation (5) results in a total ΔW_{NGI} of ~1426 km at ACT_{NGI} of 5 km and ~730-210 km with ACT_{NGI} from 10-40 km (Fig. 4a). For partial W_{NGI} uncertainties contributed from each term in Equation (5), a ±50 km of ΔW_{TGH} contributes a partial ΔW_{NGI} from ~370-180 km to ~110-65 km with ACT_{NGI} from 10-40 km using different ER and T_{TGH} values (Figs. 4b-c); a ±10 km of ΔT_{TGH} contributes a partial ΔW_{NGI} from ~260-130 km to ~70-30 km with ACT_{NGI} from 10-40 km using different W_{TGH} values (Fig. 4d); a ±0.2 mm/yr of ΔER contributes a partial ΔW_{NGI} from ~620-310 km to ~80-40 km with ACT_{NGI} from 10-40 km using different W_{TGH} values (Fig. 4e). While we interpret t as a fixed value, a ±10 Ma of Δt causes a partial ΔW_{NGI} from ~595-85 km to ~74-10 km with ACT_{NGI} from 10-40 km using different erosion rates (Fig. 4f).

3.4. Results

3.4.1. N-S size of pre-collisional NGI

Using the analyzed parameters and uncertainties with specific crustal densities and 30 myr of accretion, the mass-balance and error propagation analyses yield $W_{NGI}\pm\Delta W_{NGI}$ from 4136±1390 km to 2394±783 km with ACT_{NGI} from 5-9 km and from 2177±708 km to 707±197 km with ACT_{NGI} from 10-40 km (Fig. 5a; Table S4). A prominent issue is that W_{NGI} and ΔW_{NGI} vary significantly with different ACT_{NGI} values, whereas the ACT_{NGI} value cannot be tightly constrained. To solve this problem, we consider possible ranges of crustal accretion-involved depths for ACT_{NGI} from shallow to deep: 7-10 km, 10-15 km, 15-20 km, 20-25 km, and 30-35 km, with the reasoning for using these values discussed in following sections. These result in average W_{NGI} values based on specific ACT_{NGI} ranges, with the corresponding ΔW_{NGI} propagated from the average ΔW_{NGI} values of the specific ACT_{NGI} range and the average deviation of W_{NGI} values in the corresponding ACT_{NGI} range. Using the formula below,

$$\sigma_{a+b} = \sqrt{\sigma_a^2 + \sigma_b^2} \quad (6)$$

the average W_{NGI} at ACT_{NGI} ranges of 7-10 km, 10-15 km, 15-20 km, 20-25 km, and 30-35 km are calculated as 2564±917 km, 1815±631 km, 1348±429 km, 1093±339 km, and 821±239 km, respectively (Fig. 5a; Table S4).

3.4.2. Pre-collisional N-S size of Greater India

To determine the pre-collisional configuration of Greater India, we need to determine the original N-S width of both NGI and SGI. The relationship below calculates the original N-S width of Greater India (W_{GI}):

$$W^{GI} = W^{NGI} + W^{SGI} \quad (7)$$

W_{SGI} is relatively well-constrained as ~500-700 km from balanced cross-sections of the Lesser-Subhimalaya rocks (e.g., Robinson and Martin, 2014). Moreover, Lesser Himalayan rocks can be further extended northward because it was buried by south-directed thrusting within the TGH wedge along the MCT after ~25-20 Ma (e.g., Murphy, 2007). The magnitude of thrusting is interpreted to be ~110-220 km (Robinson et al., 2006), which represents the minimal N-S length of the unexposed Lesser Himalaya beneath the TGH. Integrating the data above, we calculate the average minimum $W_{SGI}\pm\Delta W_{SGI}$ of 736.5±99 km (Table S4). Using the W_{NGI} results above and equation (6) and (7) to calculate W_{GI} and ΔW_{GI}, the corresponding results are 3301±923 km, 2552±639 km, 2084±440 km, 1829±353 km, and 1558±259 km at ACT_{NGI} ranges of 7-10 km, 10-15 km, 15-20 km, 20-25 km, and 30-35 km, respectively (Fig. 5a; Table S4).

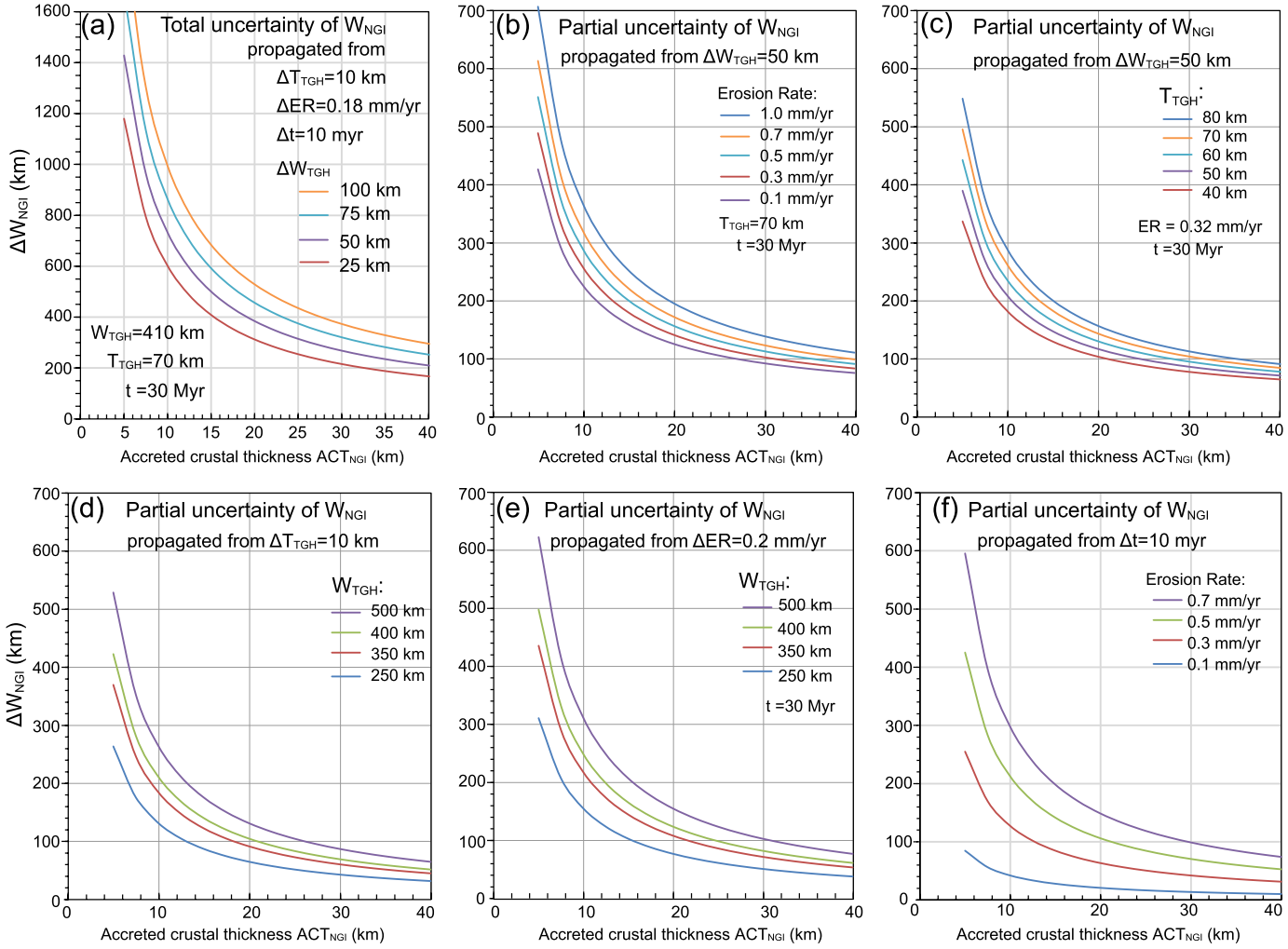

Fig. 4. Propagation of parameter uncertainties to ΔW_{NGI}. a) Total uncertainty of W_{NGI} propagated from all parameter uncertainties. b) & c) Partial contribution of W_{TGH} uncertainty to ΔW_{NGI} using different erosion rate and T_{TGH}, respectively. d) Partial contribution of T_{TGH} uncertainty to ΔW_{NGI} using different W_{TGH}. e) Partial contribution of erosion rate uncertainty to ΔW_{NGI} using different W_{TGH}. f) Partial contribution of accretion duration uncertainty to ΔW_{NGI} using different erosion rates. Parameter values are provided in Tables 1 and S1.

4. Geologic, paleomagnetic, and geodynamic evidence

The results above have not yet determined which configuration is the most likely. Therefore, constraints from geology, paleomagnetism, and geodynamics are required (Table 2).

4.1. Geologic evidence

Several primary geologic characteristics of TGH and the Gangdese arc are noteworthy:

1) TGH rocks are dominantly felsic, pelitic, and sedimentary rocks with few mafic rocks (Evidence-H1 in Table 2; Hodges, 2000; Yin, 2006);

2) Garnet Lu-Hf/Sm-Nd and monazite U-Th-Pb petrochronology document apparently successive TGH prograde metamorphism and crustal accretion-thickening from ~55-25 Ma (Evidence-H2 in Table 2; Figs. 6a-b; references in Table S5), indicating the duration of interruptions of these processes is likely shorter than the petrochronologic uncertainty of ~0.5-5 Ma;

3) Cenozoic igneous rocks in the Himalaya are dominantly S-type leucogranite from ~45-10 Ma with highly evolved Sr-Nd values, without arc-type rocks (Evidence-H3 in Table 2; Table S5; e.g., Hou et al., 2012; Wu et al., 2020);

4) Thermochronometric data from the North Himalaya domes reveal slow cooling/exhumation from ~55-25 Ma that accelerated after 25 Ma (Evidence-H4 in Table 2; Fig. 6d; Table S5; e.g., Lee et al., 2000);

5) Subsidence and flexural analyses of Late Cretaceous-Early Cenozoic Tethyan Himalayan basins document narrower foredeep and lower effective elastic lithospheric thickness (T_e of ~5-25 km) than the modern Himalayan foreland basin (T_e of ~93 km) (Evidence-H5 in Table 2; Corfield et al., 2005; DeCelles et al., 2014);

6) A consistent Paleogene sedimentary environment between the Tethyan Himalaya and Indian foreland basin requires the NGI ocean closure before ~50-45 Ma (Evidence-H6 in Table 2; DeCelles et al., 2014; Colleps et al., 2020), indicating a <1200 km NGI ocean using 120 mm/yr convergence rate (Molnar and Stock, 2009);

7) Gangdese arc-type calc-alkaline magmatism occurs continuously from ~120-100 Ma to ~30 Ma, with relatively juvenile Sr-Nd isotopic values in the ~60-30 Ma rocks (Evidence-G1 in Table 2; Fig. 6c; Table S6; e.g., Jiang et al., 2014), which require an oceanic-style mantle wedge without mid-upper crustal relamination beneath the Gangdese arc from ~60-30 Ma (e.g., Qi et al., 2021);

8) Potassic magmatism and related lower crustal xenoliths with highly evolved Sr-Nd isotopic values in Gangdese-Lhasa did not oc-

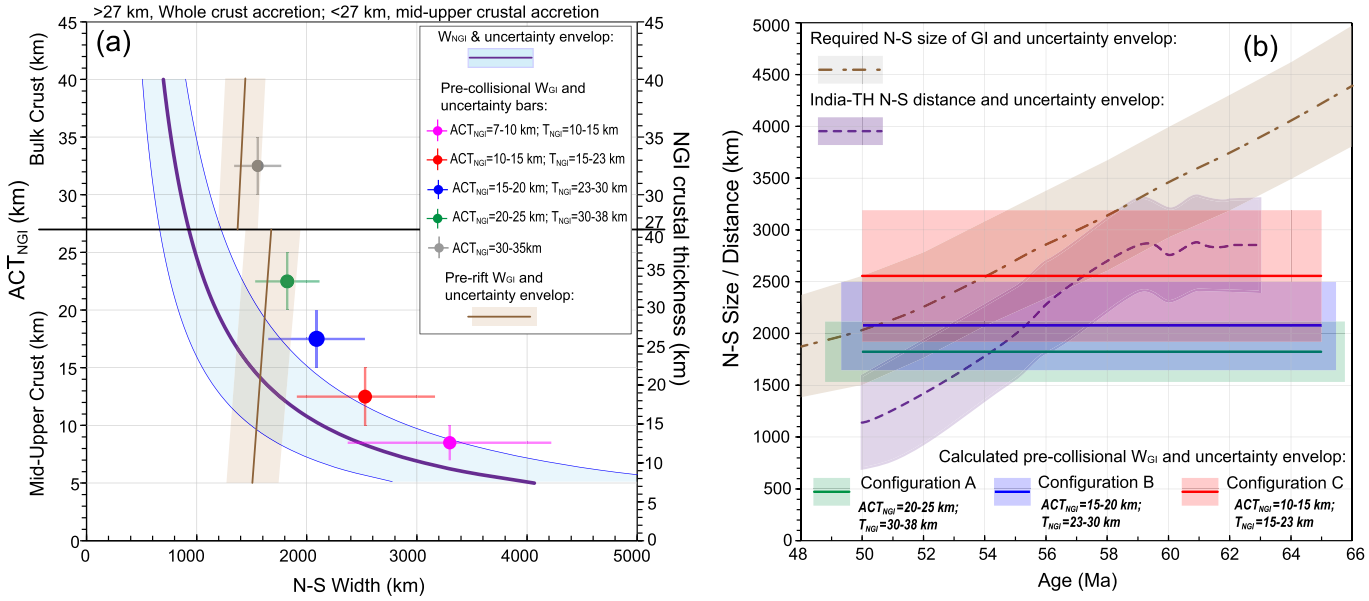

Fig. 5. a) The results from the mass-balance calculation. The blue line-shadow is the calculated W_{NGI} and uncertainty varying with ACT_{NGI}; the colored dot-bars are calculated pre-collisional W_{GI} and uncertainties using different ACT_{NGI} ranges; the brown line-shadow is the calculated pre-rift W_{GI} and uncertainty. b) Comparison between calculated results of configuration A-C and published paleolatitudes. The brown dashed line-shadow is the required Greater India size and uncertainty from published data (reference in Table S7); the purple dashed line-shadow is the distance between India and Tethyan Himalaya from published data (reference in Table S7); the green, blue, and red line-shadows are the calculated WGI and uncertainties in configurations A, B, and C. In order to facilitate the comparison, W_{GI} is assumed to be invariant with time in b).

Table 2
Compatibility between calculated configurations of Greater India and integrated evidence from Himalaya-Gangdese.

	Collision at ~ 60 Ma as precondition	Mass Balance in NGI and cross-section balance in SGI		
Evidence	Key Feature	Configuration A (1830 km wide GI, 30-38 km thick NGI)	Configuration B (2080 km wide GI, 23-30 km thick NGI)	Configuration C (> 2550 km wide GI, 10-23 km)
Paleomagnetism				
P1	India-Lhasa distance of ~5200-1550 km from ~65-30 Ma along the Yarlu suture	Require ~1200-2000 km ocean	Require ~1000-1800 km ocean	Likely ~500-1000 km ocean
P2	India-TH distance of ~2870-2090 km (±350-450 km) from ~62-56 Ma along the Yarlu suture	Require NGI ocean	Require NGI ocean	Minor or no NGI ocean
Geology				
H1	Minor mafic rock in TGH	Require mid-upper crustal accretion	Require mid-upper crustal accretion	Require mid-upper crustal accretion
H2	Continuous metamorphic ages from ~55-25 Ma in TGH	Conditional consistency due to P2	Conditional consistency due to P2	Consistent
H3	Highly evolved Nd isotopic feature of Cenozoic Himalayan granite	Conditional consistency due to P2	Conditional consistency due to P2	Consistent
H4	Slow cooling in the North Himalaya from ~55-25 Ma	Inconsistent due to predicting early Cenozoic underthrusting	Consistent	Consistent
H5	Low Te & narrow foredeep of Late Cretaceous-early Cenozoic TH foreland basin	Inconsistent	Consistent	Consistent
H6	Consistent TH-India sedimentary environment since ~50-45 Ma, indicating maximum total NGI ocean width < 1200 km	Require XBAO to be consistent	Require XBAO to be consistent	Require thrusting in EBS before 50 Ma
G1	Continuous Gangdese arc magmatism until ~30 Ma with juvenile Nd isotopic feature	Inconsistent due to predicting early Cenozoic underthrusting	Consistent	Consistent
G2	Highly evolved potassic magmatism in Gangdese-Lhasa since ~25 Ma	Inconsistent	Consistent	Consistent
G3	Slow cooling of the Gangdese arc-forearc until ~30-20 Ma followed by accelerated cooling	Inconsistent due to predicting early Cenozoic underthrusting	Consistent	Consistent
Geodynamics				
D1	Oceanic-style thinned continental NGI subduction with mid-upper crustal accretion in TGH	Inconsistent due to thick crust	Largely consistent	Consistent
D2	Thinned NGI continent with early-stage metamorphism in TGH	Inconsistent, S.A.A.	Largely consistent	Consistent
Summary				
Proposed models A, B, and C need to reconcile the independent evidence P1, P2, H6, and self-consistent H1-5, G1-3, and D1-2		Not reconciled	Conditionally reconciled	Reconciled

cur until ~25 Ma (Evidence-G2 in Table 2; Fig. 6c; Table S6) (e.g., Zhang et al., 2014; Wang et al., 2016), which requires the initial underthrusting/relaminating of the Indian mid-upper crust beneath Gangdese-Lhasa as late as ~25 Ma.

9) Thermochronometric data reveal a <5 °C/myr slow cooling history from Cretaceous time to ~30-20 Ma followed by accelerated exhumation in both the Gangdese arc plutons and the Xigaze forearc basin (Evidence-G3 in Table 2; Fig. 6d; reference in Ta-

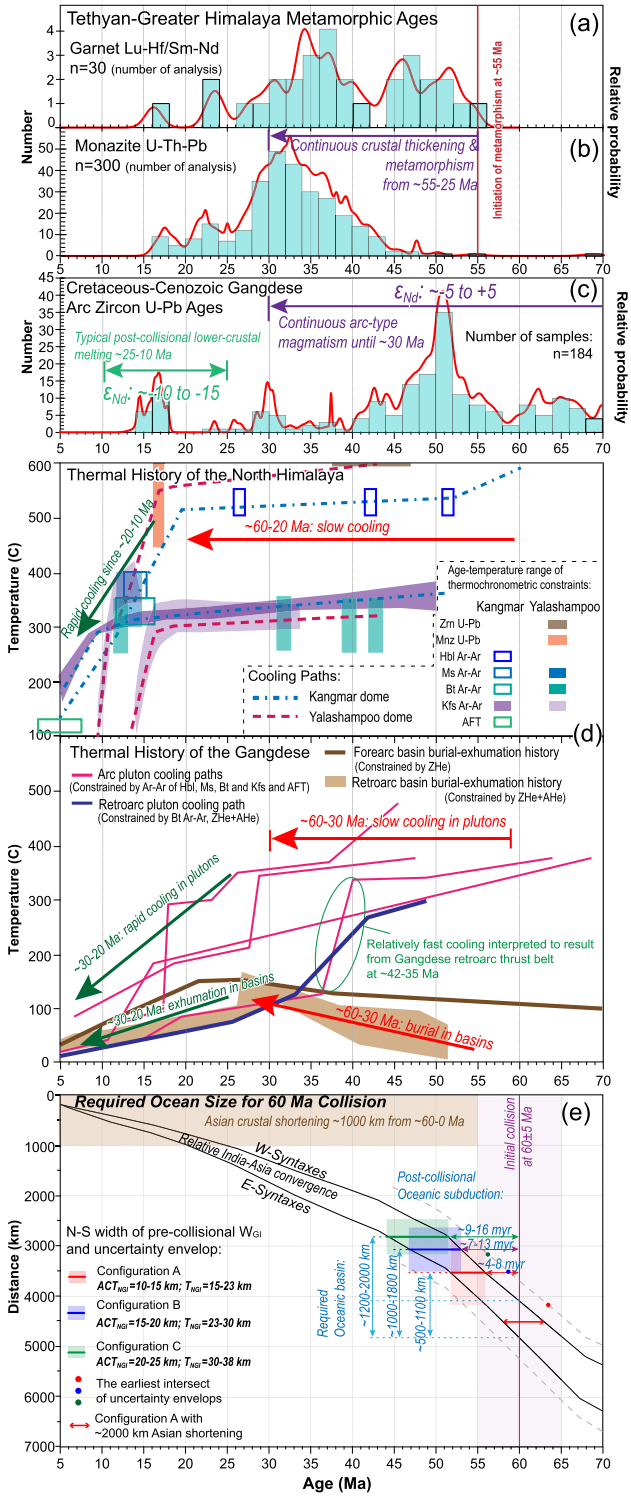

Fig. 6. Integrated evidence from regional geology and paleomagnetism. a) & b) Metamorphic age distribution of the Tethyan-Greater Himalaya using garnet-whole rock Lu-Hf & Sm-Nd and monazite U-Th-Pb petrochronology (references in Table S5). c) Age distribution and corresponding ε_{Nd} value ranges of the Gangdese arc (reference in Table S6). d) Cooling histories of the Gangdese arc, forearc, and retroarc (references in Table S6) and North Himalaya (Lee et al., 2000) indicating slow cooling until ~30-20 Ma followed by accelerated cooling. e) Required oceanic basin sizes from the comparison between the results from mass-balance analysis and relative India-Asia convergence. The brown shadow is the Cenozoic shortening magnitude in Asia (reference in Table S1); the two black lines are relative convergence at W- and E-sytaxes (data from Van Hinsbergen et al., 2011b); the gray dashed-lines are the margins of uncertainty envelops of relative convergence; the green, blue, and red line-shadows are the calculated WGI and uncertainties in configurations A, B, and C; the blue dashed lines are reference lines without geologic significance.

ble S6), indicating a dynamic shift from weak-coupling to strong-coupling between the overriding and downgoing plates at ~30-20 Ma.

4.2. Paleomagnetic evidence

Paleomagnetic studies yield prominent paleolatitude gaps between South Tibet and India and between the Tethyan Himalaya and northern India. Paleolatitude gaps between South Tibet and cratonic India along the Yarlu suture vary from ~45-14° from ~65-30 Ma, corresponding to distances of ~5000-1550 km (Evidence-P1 in Table 2; Van Hinsbergen et al., 2012). The uncertainties are ~ ±2.4-4.1° for Greater India and ~ ±2.2-3.9° for South Tibet (Table S7), indicating the propagated uncertainties of ~ ±360-630 km using equation (7). Moreover, previous studies indicate paleolatitude gaps between Tethyan Himalaya and cratonic India along the Yarlu suture vary from ~6.5-15.9° from ~75-68 Ma, ~15.0-25.9° from ~63-59 Ma, ~15.1-20.3° from ~59-56 Ma, and ~17.9-10.4 from ~55-50 Ma (Evidence-P2 in Table 2; reference in Table S7).

4.3. Geodynamic evidence

The mass-balance analysis cannot determine whether the proposed NGI configurations are permissible in geodynamic models of the India-Asia collision. However, two representative geodynamic studies illustrate the dynamic processes of NGI convergence in relation to the NGI configuration.

Capitanio et al. (2010) find that an extended ~5-15 km thick mafic lower crust and a ~70 km thick NGI mantle lithosphere with a ~10-20 km thick buoyant mid-upper crust scraped-off at the Himalayan front can continuously conduct a mature oceanic-style continental subduction, with the duration and velocity history consistent with the observed Early Cenozoic Indian plate velocity history (Evidence-D1 in Table 2). Their study also finds that subduction with either an unextended mafic lower crust or an extended lithosphere including mid-upper crust would stall the subduction, inconsistent with the Cenozoic velocity history.

Kelly et al. (2022) study the geodynamic processes coeval with Early Cenozoic TGH accretion. Their models require a 1000 km N-S wide NGI with a northward thinning bulk crustal thickness from 36-6 km and mid-upper crustal thickness from 24-4 km, equivalent to average bulk and mid-upper crustal thickness of NGI of 21 km and 14 km, respectively (Evidence-D2 in Table 2). The northward thinning causes the convergence to change from the early-stage steep subduction with NGI mafic lower crustal eclogitization to the late-stage shallow underthrusting, with plate-coupling from weak to strong. In their models, these processes are coeval with mid-upper NGI crustal accretion and regional metamorphism in the TGH from 55-45 Ma.

In summary, both geodynamic studies favor a pre-collisional NGI configuration with a thinned <25 km average crustal thickness. Based on their models, the thinned NGI crust can conduct crustal accretion of the mid-upper crust coeval with oceanic-style subduction of the lower crust and mantle lithosphere.

5. Interpretation and discussion

5.1. Pre-collisional NGI crustal thickness in mass balance

To analyze the NGI pre-collisional configuration, we need to know the average NGI crustal thickness corresponding to specific W_{NGI}. In mass-balance analysis, we used the average thickness of the accreted NGI crustal layer, ACT_{NGI}, which does not necessarily equal the thickness of any specific architectural layer of NGI crust.

However, other lines of evidence listed above provide a relationship between crustal thickness and ACT_{NGI}.

The TGH lithologies (H1 in Table 2) indicate that TGH accretion probably did not involve significant NGI mafic lower crust. Moreover, the subduction from ~60-30 Ma likely did not involve significant NGI mid-upper crust. As the Rayleigh-Taylor instability would cause the relamination of subducted mid-upper crust in the upper plate, causing highly evolved Sr-Nd isotopic values in the coeval Gangdese magma, inconsistent with juvenile isotopic features from ~60-30 Ma with subsequent evolved features after 25 Ma in the Gangdese arc (G1-2 in Table 2). These three lines of evidence indicate that the ACT_{NGI} equals the NGI mid-upper crustal thickness (MUT_{NGI}), with the mafic lower crust subducted, consistent with geodynamic results that plate velocity history requires Indian mafic lower crustal subduction and mid-upper crustal accretion (D1 in Table 2). Considering a 3-layer crust with equal thicknesses of each layer, an average NGI crustal thickness (T_{NGI}) and/or MUT_{NGI} can directly substitute for ACT_{NGI} in equation (4):

$$ACT_{NGI} = MUT_{NGI} = \frac{2}{3}T_{NGI} \quad (8)$$

The combination of equations (4) and (8) provides a relationship between N-S width and average crustal thickness of NGI.

Current crustal thicknesses are ~35-40 km for the northern Indian craton and 38.8±6.2 km for Australia, which we interpret to represent the maximum NGI crustal thickness (Clitheroe et al., 2000; Gupta et al., 2003). A maximum of ~40 km thick crust indicates a mid-upper crustal thickness up to ~27 km. TGH lithologies (H1 in Table 2) indicate that an $ACT_{NGI} = MUT_{NGI} > 27$ km requiring lower crust accretion is unlikely and not discussed further. Moreover, we use 10 km as the lower T_{NGI} limit, as a continental crustal thickness is unlikely <10 km. These indicate that the ACT_{NGI} or MUT_{NGI} value ranges of ~7-10 km, ~10-15 km, 15-20 km, and 20-25 km in Section 3 reasonably cover a broad range of possible T_{NGI} from ~10-15 km, 15-23 km, 23-30 km, to 30-38 km (Fig. 5a).

5.2. The configuration of NGI and Greater India from mass-balance

While the W_{NGI} uncertainties with an $ACT_{NGI} < 10$ km or $T_{NGI} < 15$ km are ~1400-800 km, the magnitude of uncertainties using ACT_{NGI} from ~10-25 km or T_{NGI} from ~15-38 km is considerably less at ~700-300 km (Fig. 5a; Table S4), corresponding to latitudes of ~2.7-6.3°. This range is within general uncertainty ranges of ~2-10° from paleomagnetism (i.e., Van Hinsbergen et al., 2012), which indicates that a W_{NGI} at T_{NGI} from ~15-38 km is permissible and warrants primary discussion.

Considering the proposed T_{NGI} above, the calculated W_{NGI} from mass-balance and the structurally restored ~736 km wide unextended SGI provide three possible types of pre-collisional Greater Indian (GI) configurations with a distal NGI from thick-narrow to thin-wide: A) ~1830±350 km wide GI with ~1093 km wide and ~30-38 km thick NGI; B) ~2080±440 km wide GI with ~1348 km wide and ~23-30 km thick NGI; C) ~2550±640 km wide GI with ~1815 km wide and ~15-23 km thick NGI (Figs. 5a, 7; Table S4). Moreover, a thinner ~10-15 km thick NGI crust yields ~3301±922 km wide GI and ~2564±917 km wide NGI, with larger uncertainties (Fig. 5a; Table S4).

5.3. Paleolatitude comparison

We determine whether the proposed configurations are compatible with the paleolatitudes (Tables 2, S7). The paleolatitudes indicate India-Tethyan Himalaya (TH) distances of ~2875-1990 km from ~62-55 Ma with uncertainties from ~ ±340-640 km (Table S7; purple dashed-line and shadow in Fig. 5b). Configuration A and B with an ~1830±350 km (green line-shadow in Fig. 5b) and an ~2080±440 km GI (blue line-shadow in Fig. 5b), respectively, show less overlap with the distance envelope. Both configurations with shorter and thicker NGI crust require an >500-1000 km NGI oceanic basin to match the India-TH latitude gap from 62-55 Ma (Fig. 5b). However, configuration C with an ~2550±640 km GI (red line-shadow in Fig. 5b) closely matches the India-TH distances, indicating no need for a >500 km NGI oceanic basin.

The relative India-Asia distances from paleomagnetism provide the required GI size for initial collision at specific times (Fig. 6e). The India-Asia distance along the Yarlu suture from ~66-48 Ma is ~4960-2570 km and ~5820-3180 km at the western and eastern Himalaya syntaxes, respectively (Table S7; Van Hinsbergen et al., 2011b). The E-W deviation of distances with a minimal ±2.5° paleomagnetic uncertainty indicate a combined uncertainty of ±580-500 km for the required GI size (Table S7). Due to relatively large >500 km uncertainties, we interpret the earliest intersections of uncertainty envelopes between configurations A-C and required GI size to represent the ***possible*** initial timing of collision, with the intersections of median lines to represent the ***likely*** timing of collision (Figs. 5b, 6e). Using the average India-Asia distances with a fixed ~1000 km Cenozoic internal shortening in Asia, the required GI size is ~4390-1880 km from 66-48 Ma (brown dashed-line and shadow in Fig. 5b). The median lines of W_{GI} in configurations A-C intersect with the required GI sizes at ~48 Ma, ~50.5 Ma, and ~54 Ma, with the earliest intersections of uncertainty envelops at ~54 Ma, ~57 Ma, and ~62 Ma, respectively (Fig. 5b). Alternatively, by adding ~1000 km of Asian shortening and ±400 km paleolatitude uncertainty, the median lines of W_{GI} in configurations A-C intersect with the relative India-Asia distances at the two Himalayan syntaxes (black-lines in Fig. 6e; Table S7) at 51-45 Ma, 53-47 Ma, and 56-52 Ma, respectively, with the earliest intersection of uncertainty envelops at ~56 Ma, ~58-59 Ma, and ~63-64 Ma, respectively (Fig. 6e). Therefore, configurations A-C permit an initial collision at ~56-48 Ma, ~58-51 Ma, and ~63-54 Ma, respectively, assuming no additional oceanic basin (Fig. 6e).

If we consider the broadly-accepted initial collision timing at 60±5 Ma (e.g., Ding et al., 2022), oceanic basins are likely required, with a ~1200-2000 km and ~1000-1800 km oceanic basins for configurations A and B, and a ~500-1100 km smaller oceanic basin for configuration C and, respectively (Fig. 6e; Table 2). However, considering the intersections of uncertainty envelopes, only configuration C has a possible ~60 Ma initial collision timing without an additional oceanic basin.

5.4. Compatibility between evidence and incorporated oceanic basins

Previous studies have proposed two endmember models with oceanic basins: the Greater Indian Oceanic Basin (GIB) in NGI (Fig. 1a), and Xigaze Back-Arc Oceanic Basin (XBAO) in southern Asia (Fig. 1b). These models are proposed to compensate for the continental width deficits for the ~60 Ma initial collision (Fig. 7).

5.4.1. Oceanic basin in NGI

In GIB model, configuration A-B with a >1000 km NGI oceanic basin predicts a period of oceanic subduction between 60 Ma and 30 Ma with a >8 myr interruption of TGH accretion (Fig. 8a), considering an ~120 mm/yr subduction rate (Molnar and Stock, 2009). This prediction is not consistent with apparently continuous crustal thickening and the absence of subduction-related magmatism in the TGH from ~60-30 Ma (H2-3 in Table 2). Moreover, a southward shift of the subduction zone between TGH and India would terminate arc-type magmatism in the Gangdese arc after 60 Ma (Fig. 8a), inconsistent with continuous Gangdese arc magmatism from ~60-30 Ma (G1 in Table 2). Therefore, configurations A

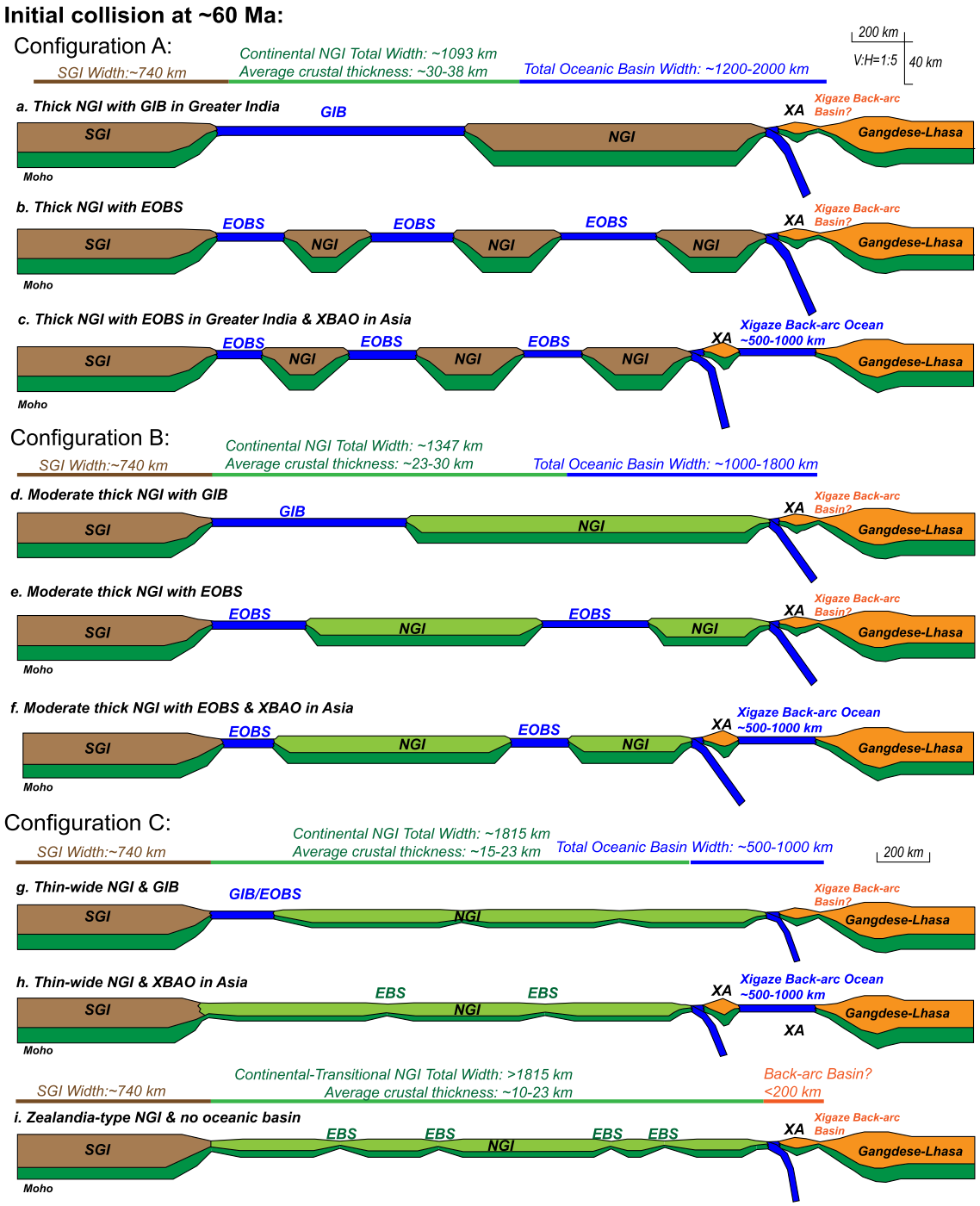

Fig. 7. Proposed configurations of NGI with collision at ~60 Ma. Configuration A: a) Greater India oceanic basin (GIB), b) extensional NGI oceanic basin system (EOBS), and c) Xigaze back arc oceanic basin (XBAO) with EOBS in a ~1093 km wide and ~30-38 km thick NGI. Configuration B: d) GIB, e) EOBS, and f) XBAO with EOBS in a ~1348 km wide and ~23-30 km thick NGI. Configuration C: g) Limited GIB or EOBS, h) XBAO in an ~1815 km wide and ~15-23 km thick hyper-extended NGI, and i) Zealandia-type continent without oceanic basin in a >1815 km wide and ~10-23 km thick hyper-extended NGI. XA: Xigaze arc. EBS: Extensional basin system.

and B with a large GIB are inconsistent with geological evidence (Figs. 7a, 7d; Table 2).

Alternatively, a single large GIB can be separated to several small <500 km extensional oceanic basin systems (EOBS) in configurations A and B, with discrete continental crustal strips within NGI (Figs. 7b, 7e). In this scenario, post-collisional subduction of an individual oceanic basin only causes <5 Myr of interruption in TGH accretion-thickening, which may not be detectable in petrochronology due to analytical uncertainties of ~0.5-5 Ma (H2 in Table 2). However, an EOBS suggests post-collisional subduction initiation within NGI (Fig. 8a-b) and predicts either 1) formation of simultaneous subduction-related magmatism within 1-2 myr (Ishizuka et al., 2011; Maunder et al., 2020) or 2) accretion of oceanic upper crust without subduction-related magmatism (McCarthy et al., 2018), inconsistent with absence of subduction-related magma and minor volumes of mafic rock in the TGH (H3&H1 in Table 2), respectively.

Otherwise, we must assume no subduction initiation in an EOBS after the initial collision. However, configuration A with an

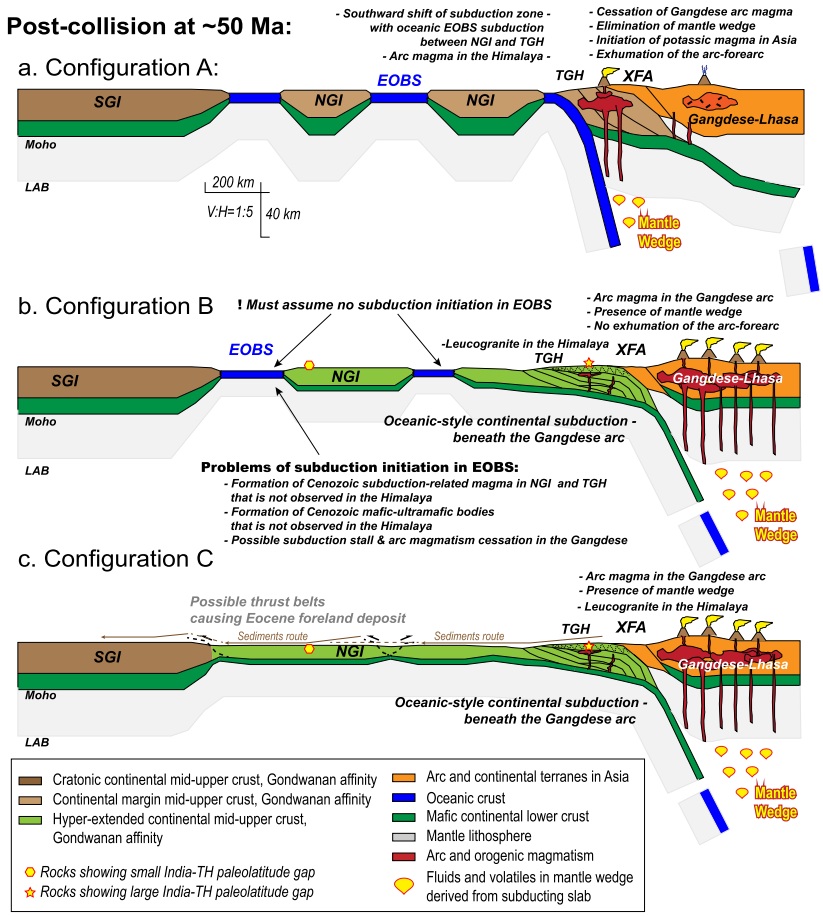

Fig. 8. Predicted post-collisional evolution of the proposed NGI configurations at ~50 Ma. a) thick-narrow configuration A; b) moderate thick configuration B; and c) thin-wide configuration C. XFA: Xigaze forearc; LAB: lithosphere-asthenosphere boundary.

EOBS and thick crust >30 km (Fig. 7a-b) predicts subduction zone congestion beneath the Gangdese arc based on geodynamic results (D1 in Table 2), causing the cessation of arc-type magma, initiating potassic magmatism after 60 Ma, and forcing the southward shift of the subduction zone within the EOBS (Fig. 8a). These are inconsistent with ~60-30 Ma continuous arc-type magmatism followed by potassic magmatism after ~25 Ma in Gangdese arc with coeval absence of subduction-related magmatism in TGH (G1, G2, and H3 in Table 2). Moreover, configuration A predicts periodic collision of relatively thick NGI continental crustal strips, with periodic exhumation in the Gangdese arc, forearc, and/or North Himalaya, inconsistent with the low-magnitude of exhumation in both North Himalaya and Gangdese arc from ~60-30 Ma (H5&G3 in Table 2; Fig. 6d). In addition, configuration A requiring an ~1200-2000 km wide total NGI ocean is inconsistent with the maximum NGI ocean width of <1200 km based on the interpreted spatially connected sedimentary environment between TH and India since ~50 Ma (H6 in Table 2). These data indicate configuration A with either GIB or EOBS is unlikely.

For configuration B with an EOBS (Fig. 7e) and configuration C with either a small GIB or EOBS (Fig. 7g), the thinner crusts are permissible to conduct continuous TGH accretion and oceanic-style continental subduction beneath the Gangdese arc in geodynamic models (D1-2 Table 2). Continuous subduction without congestion probably predicts insignificant intraplate compression without a southward shift of induced subduction initiation within NGI (Stern and Gerya, 2018), which allows both configurations to be consistent with most geologic evidence (Table 2). However, this interpretation still requires further geodynamic studies to verify. Moreover, a >100-200 km (1-2 Myr × 120 mm/yr) NGI oceanic lithosphere is problematic, as oceanic crustal fragment and/or subduction-related sedimentary rocks are not found in the well-exposed TGH.

5.4.2. Oceanic basin in Asia

A >1000 km oceanic basin between the Xigaze and Gangdese arcs in XBAO model enlarges the magnitude of internal convergence in Asia to >2000 km, causing the initial collision to be between NGI and Xigaze arc (Figs. 7c, f, h) (Cai et al., 2011; Kapp and DeCelles, 2019). The XBAO hypothesis predicts post-collisional oceanic subduction between the Xigaze and Gangdese arcs, with early-stage TGH accretion and regional metamorphism involved in an arc-continental collision. The ~50 Ma early-stage TGH regional metamorphism occurs across a >100 km wide region (Smit et al., 2014; Lihter et al., 2022). In contrast, the metamorphic belts in typical arc-continent collision, i.e., Timor and New Guinea, occur much narrower <50 km width and shorter <10 Myr duration of metamorphism (Cloos et al., 2005; Harris, 2011). These indicate that the TGH regional metamorphism <50-45 Ma was unlikely formed in an arc-continental collision setting, indicating the arc-continent collision with XBAO closure no later than 50 Ma, further suggesting a maximum XBAO size of ~1200 km (~10 Myr × 120 mm/yr).

The gap between the required GI size and the India-TH distance based on paleolatitudes defines the size of XBAO, which is ~500-1100 km from ~62-50 Ma (Fig. 5b). Noticeably, the TH paleolatitudes only represent a minimum approximation of original northern TH margin, indicating that the India-TH paleolatitude gap represents the minimum GI size (Fig. 5b) and the ~500-1100 km to be the maximum XBAO size. Therefore, additional EOBS in NGI are still likely required to coexist with an XBAO in configurations

A and B for a 60 Ma collision (Figs. 7c, f) based on their required ocean sizes of ~1200-2000 km and ~1000-1800 km, respectively (Fig. 6e). The required EOBS sizes are ~700-1000 km and ~500-800 km, respectively. As stated above, configuration A involving EOBS is unlikely; therefore, we exclude configuration A (Figs. 7a-c).

For configuration B with a relatively thin ~23-30 km crust and coexisting XBAO and EOBS (Fig. 7f), it predicts ~4-8 myr of XBAO subduction after an ~60 Ma collision followed by a continued oceanic-style subduction of both the NGI continent and EOBS beneath the Gangdese arc since ~56-52 Ma based on geodynamic studies (D1-2 in Table 2; Fig. 8b). These further predict a limited foredeep width and low-magnitude of plate-coupling between NGI and overriding Gangdese arc-forearc, and keep a mantle wedge beneath the Gangdese for arc-type magma coeval with apparently continuous mid-upper crustal accretion in TGH from ~60-30 Ma, consistent with the primary geologic features in both the TGH (H2&H4-6 in Table 2) and Gangdese arc (G1-3 in Table 2). However, to be consistent with the coeval absence of subduction-related magmatism and insignificant volume of mafic rocks in the TGH (H1&H3 in Table 2), we must assume no post-collisional subduction initiation in EOBS without EOBS crustal accretion in TGH. This assumption leads to configuration B with a ~500-800 km EOBS in NGI and ~500-1000 km XBAO in Asia (Fig. 7f, 8b) conditionally consistent with most of the evidence, which conditionally supports a combination of previous two-stage models (Cai et al., 2011; Van Hinsbergen et al., 2012; Kapp and DeCelles, 2019).

Configuration C has the widest W_{NGI} of ~1815 km and W_{GI} of ~2550 km with the thinnest crustal thickness of 15-23 km, and incorporates a ~500-1000 km XBAO, allowing an ~60 Ma or earlier initial collision, with an additional NGI oceanic basin and related assumptions not needed (Figs. 6e, 7h). Configuration C predicts post-collisional geologic processes similar to configuration B based on geodynamic results (D1-2 in Table 2; Fig. 8c), and is more consistent with all lines of geologic evidence (H1-6&G1-3 in Table 2) than configuration B. This scenario predicts an approximate single-stage Paleocene collision due to short-term ~4-8 Myr post-collisional XBAO oceanic subduction. However, the problem is that the evidence indicating the presence of XBAO is insufficient (Cai et al., 2011; Ding et al., 2022). Alternatively, a possible larger Lhasa-Qiangtang-Tarim convergence (Song et al., 2022) would double the Cenozoic Asian crustal shortening to ~2000 km, resulting in an ~63-58 Ma collision for configuration C without needing an oceanic basin (Fig. 6e).

5.5. Hyper-extended NGI, an alternative scenario for single-stage collision?

Zealandia provides a modern analog for NGI in configuration C. The N-S trending Zealandia shows an E-W width of ~1200-2400 km with the average crustal thickness varying from ~12-24 km (Klingelhoefer et al., 2007; Grobys et al., 2008; Gallais et al., 2019). The calculated NGI width of ~1815 km with an average thickness of ~15-23 km is compatible with these features. Zealandia shows a rise-trough configuration largely within a continental crust, with ~200-600 km wide and ultra-thinned 10-15 km continental or transitional crust in extensional troughs or basins (Klingelhoefer et al., 2007). This indicates that the continental crust can be further stretched without forming significant oceanic lithosphere (Grobys et al., 2008) (Fig. 7i). Incorporating an ~10-15 km thick continental crust, the mass-balance analysis results in a maximum ~2560 km wide NGI and ~3300 km wide GI (Fig. 5a). The width is largely within the uncertainty of configuration C and broadly matches the required GI size for ~60 Ma collision (Figs. 5a-b), supporting a single-stage collision hypothesis (e.g., Cai et al., 2011; Ding et al., 2005, 2022).

Instead of assuming oceanic basins in NGI or Asia (Fig. 7i), a Zealandia-type NGI requires significant Cretaceous continental extension. Abundant ~147-115 Ma mafic intrusions in the Tethyan Himalaya directly indicate NGI continental extension in Late Jurassic-Early Cretaceous time (e.g., Chen et al., 2018). Moreover, paleomagnetic studies suggest Cretaceous GI size of ~2000-2700 km at ~137-125 Ma, indicating large extensional magnitudes in NGI (Meng et al., 2020). In particular, both geologic and geodynamic evidence of post-collisional Himalaya-Gangdese (Table 2) require a $T_{NGI}<25$ km, resulting in a pre-collisional $W_{GI}>2150$ km in the mass-balance analysis (Figs. 5a; Table S4), consistent with the paleomagnetic results. These further raise the possibility that a hyper-extended Zealandia-type NGI formed broadly coeval with internal extension in Zealandia (Hoernle et al., 2020). Geodynamic modeling of diffuse continental extension with Moho temperature >780 °C during NE Gondwanan breakup (Huerta and Harry, 2007) demonstrates the formation of hyper-extended terranes without much oceanic lithosphere.

5.6. Pre-rift Greater India and post-collisional shortening

Using a 40 km crustal thickness for pre-rift Greater India, the width of pre-rift NGI can be calculated. The results indicate a ~636-946 km wide pre-extension NGI, resulting in a 1370-1680 km wide pre-rift Greater India (Fig. 5a; Table S4). We interpret that 1) an E-W trending pre-rift Greater India leads paleomagnetism to not confine its pre-rift N-S size; and 2) 3D continental extensional tectonic models indicate the Wallaby-Zenith fractural zone is likely a transfer zone within an extensional system, which is less likely to confine NGI (Fig. S1). Moreover, the Late Jurassic oceanic crustal sliver in Gibbons et al. (2012) could be a portion of the Jurassic NGI internal extensional basin (Fig. S1), not necessarily indicating a broad ocean. Therefore, a ~1400-1700 km pre-rift Greater India reaching the southern Exmouth plateau as suggested by Powell et al. (1988) is likely.

Both configurations B and C predict large magnitudes of >1000 km crustal shortening coeval with TGH accretion, further predicting that the early-stage Himalaya was dominated by ductile duplexing (Webb et al., 2007). Recently recognized Greater Himalayan ductile discontinuities (e.g., Carosi et al., 2018) are likely the structure that accommodated this convergence (Figs. 8c-d). While the magnitude of this shortening is poorly defined, currently determined timing of motion on these discontinuities from ~40-25 Ma (Carosi et al., 2018) is broadly consistent with the duration of TGH accretion.

6. Conclusions

Mass-balance analysis combined with geologic, paleomagnetic, and geodynamic evidence indicate two possible types of Northern Greater India configurations prior to the ~60 Ma collision:

1) A ~2080 km wide Greater India with a less stretched ~23-30 km thick NGI requires ~500-1000 km oceanic basin systems in both Asia and NGI, which predicts a multi-stage collision since ~60 Ma with short-term post-collisional oceanic subduction, conditionally consistent with the integrated evidence.

2) A ≥2550 km wide Greater India with a hyper-extended ~10-23 km thick Zealandia-type NGI without or with limited ~500-1000 km Xigaze backarc oceanic basin predicts an approximate single-stage collision at ~60 Ma followed by oceanic-style post-collisional continental subduction, consistent with the integrated evidence.

CRediT authorship contribution statement

Yipeng Li: Conceptualization, Formal analysis, Investigation, Methodology, Writing – original draft, Writing – review & edit-

ing. **Delores M. Robinson:** Conceptualization, Funding acquisition, Investigation, Methodology, Project administration, Supervision, Writing – review & editing.

Declaration of competing interest

The authors declare that they have no known competing financial interests or personal relationships that could have appeared to influence the work reported in this paper.

Data availability

I have shared in attachment.

Acknowledgements

This research is supported by NSF award of EAR-2020444 for DMR. YL is grateful for the Postdoctoral Fellowship 514286 funded by the College of Arts and Sciences at the University of Alabama. The authors thank Dr. Alex Webb for editorial handling and four anonymous reviewers for their constructive and insightful review. The first author thanks Drs. Lin Ding at ITPCAS and Alexander Robinson at UH for introducing and inspiring him to study tectonics in Tibetan Plateau. The first author also thanks Drs. Fulong Cai, Liyun Zhang, Houqi Wang, Peiping Song, and Chao Wang at ITPCAS for their thoughtful discussions in South Tibet and Gangdese geology and paleomagnetism.

Appendix A. Supplementary material

Supplementary material related to this article can be found online at https://doi.org/10.1016/j.epsl.2023.118098.

References

Aikman, A.B., Harrison, T.M., Hermann, J., 2012. The origin of Eo- and Neo-himalayan granitoids, Eastern Tibet. J. Asian Earth Sci. 58, 143–157.
Cai, F., Ding, L., Yue, Y., 2011. Provenance analysis of upper Cretaceous strata in the Tethys Himalaya, southern Tibet: implications for timing of India–Asia collision. Earth Planet. Sci. Lett. 305 (1–2), 195–206.
Capitanio, F.A., Morra, G., Goes, S., Weinberg, R.F., Moresi, L., 2010. India–Asia convergence driven by the subduction of the Greater Indian continent. Nat. Geosci. 3 (2), 136–139.
Carosi, R., Montomoli, C., Iaccarino, S., 2018. 20 years of geological mapping of the metamorphic core across Central and Eastern Himalayas. Earth-Sci. Rev. 177, 124–138.
Chen, S.S., Fan, W.M., Shi, R.D., Liu, X.H., Zhou, X.J., 2018. 118–115 Ma magmatism in the Tethyan Himalaya igneous province: constraints on Early Cretaceous rifting of the northern margin of Greater India. Earth Planet. Sci. Lett. 491, 21–33.
Christensen, N.I., Mooney, W.D., 1995. Seismic velocity structure and composition of the continental crust: a global view. J. Geophys. Res., Solid Earth 100 (B6), 9761–9788.
Clitheroe, G., Gudmundsson, O., Kennett, B.L.N., 2000. The crustal thickness of Australia. J. Geophys. Res., Solid Earth 105 (B6), 13697–13713.
Cloos, M., Sapiie, B., van Ufford, A.Q., Weiland, R.J., Warren, P.Q., McMahon, T.P., 2005. Collisional delamination in New Guinea: the geotectonics of subducting slab breakoff. GSA Special Paper 400.
Colleps, C.L., McKenzie, N.R., Horton, B.K., Webb, A.A.G., Ng, Y.W., Singh, B.P., 2020. Sediment provenance of pre- and post-collisional Cretaceous–Paleogene strata from the frontal Himalaya of northwest India. Earth Planet. Sci. Lett. 534, 116079.
Corfield, R.I., Watts, A.B., Searle, M.P., 2005. Subsidence history of the north Indian continental margin, Zanskar–Ladakh Himalaya, NW India. J. Geol. Soc. 162 (1), 135–146.
Cowgill, E., Forte, A.M., Niemi, N., Avdeev, B., Tye, A., Trexler, C., Godoladze, T., 2016. Relict basin closure and crustal shortening budgets during continental collision: an example from Caucasus sediment provenance. Tectonics 35 (12), 2918–2947.
DeCelles, P.G., Kapp, P., Gehrels, G.E., Ding, L., 2014. Paleocene-Eocene foreland basin evolution in the Himalaya of southern Tibet and Nepal: implications for the age of initial India-Asia collision. Tectonics 33 (5), 824–849.
DeCelles, P.G., Robinson, D.M., Zandt, G., 2002. Implications of shortening in the Himalayan fold-thrust belt for uplift of the Tibetan Plateau. Tectonics 21 (6), 1–12.
Ding, L., Kapp, P., Wan, X., 2005. Paleocene–Eocene record of ophiolite obduction and initial India-Asia collision, south central Tibet. Tectonics 24 (3).
Ding, L., Kapp, P., Cai, F., Garzione, C.N., Xiong, Z., Wang, H., Wang, C., 2022. Timing and mechanisms of Tibetan Plateau uplift. Nat. Rev. Earth Environ., 1–16.
Ding, L., Qasim, M., Jadoon, I.A., Khan, M.A., Xu, Q., Cai, F., Yue, Y., 2016. The India–Asia collision in north Pakistan: insight from the U–Pb detrital zircon provenance of Cenozoic foreland basin. Earth Planet. Sci. Lett. 455, 49–61.
Ding, L., Spicer, R.A., Yang, J., Xu, Q., Cai, F., Li, S., Mehrotra, R., 2017. Quantifying the rise of the Himalaya orogen and implications for the South Asian monsoon. Geology 45 (3), 215–218.
Gallais, F., Fujie, G., Boston, B., Hackney, R., Kodaira, S., Miura, S., Kaiho, Y., 2019. Crustal structure across the Lord Howe Rise, northern Zealandia, and rifting of the eastern Gondwana margin. J. Geophys. Res., Solid Earth 124 (3), 3036–3056.
Gibbons, A.D., Barckhausen, U., Van Den Bogaard, P., Hoernle, K., Werner, R., Whittaker, J.M., Müller, R.D., 2012. Constraining the Jurassic extent of Greater India: tectonic evolution of the West Australian margin. Geochem. Geophys. Geosyst. 13 (5).
Grobys, J.W., Gohl, K., Eagles, G., 2008. Quantitative tectonic reconstructions of Zealandia based on crustal thickness estimates. Geochem. Geophys. Geosyst. 9 (1).
Gupta, S., Rai, S.S., Prakasam, K.S., Srinagesh, D., Bansal, B.K., Chadha, R.K., Gaur, V.K., 2003. The nature of the crust in southern India: implications for Precambrian crustal evolution. Geophys. Res. Lett. 30 (8).
Harris, R., 2011. The nature of the Banda Arc–continent collision in the Timor region. In: Arc-Continent Collision. Springer, Berlin, Heidelberg, pp. 163–211.
Hodges, K.V., 2000. Tectonics of the Himalaya and southern Tibet from two perspectives. Geol. Soc. Am. Bull. 112 (3), 324–350.
Hoernle, K., Timm, C., Hauff, F., Tappenden, V., Werner, R., Jolis, E.M., Gohl, K., 2020. Late Cretaceous (99-69 Ma) basaltic intraplate volcanism on and around Zealandia: tracing upper mantle geodynamics from Hikurangi Plateau collision to Gondwana breakup and beyond. Earth Planet. Sci. Lett. 529, 115864.
Huerta, A.D., Harry, D.L., 2007. The transition from diffuse to focused extension: modeled evolution of the West Antarctic Rift system. Earth Planet. Sci. Lett. 255 (1–2), 133–147.
Hu, X., Garzanti, E., Moore, T., Raffi, I., 2015. Direct stratigraphic dating of India-Asia collision onset at the Selandian (middle Paleocene, 59±1 Ma). Geology 43 (10), 859–862.
Hou, Z.Q., Zheng, Y.C., Zeng, L.S., Gao, L.E., Huang, K.X., Li, W., Sun, Q.Z., 2012. Eocene–Oligocene granitoids in southern Tibet: constraints on crustal anatexis and tectonic evolution of the Himalayan orogen. Earth Planet. Sci. Lett. 349, 38–52.
Ingalls, M., Rowley, D.B., Currie, B., Colman, A.S., 2016. Large-scale subduction of continental crust implied by India–Asia mass-balance calculation. Nat. Geosci. 9 (11), 848–853.
Ishizuka, O., Tani, K., Reagan, M.K., Kanayama, K., Umino, S., Harigane, Y., Dunkley, D.J., 2011. The timescales of subduction initiation and subsequent evolution of an oceanic island arc. Earth Planet. Sci. Lett. 306 (3–4), 229–240.
Jiang, Z.Q., Wang, Q., Wyman, D.A., Li, Z.X., Yang, J.H., Shi, X.B., Guo, H.F., 2014. Transition from oceanic to continental lithosphere subduction in southern Tibet: evidence from the Late Cretaceous–Early Oligocene (∼ 91–30 Ma) intrusive rocks in the Chanang–Zedong area, southern Gangdese. Lithos 196, 213–231.
Kapp, P., DeCelles, P.G., 2019. Mesozoic–Cenozoic geological evolution of the Himalayan-Tibetan orogen and working tectonic hypotheses. Am. J. Sci. 319 (3), 159–254.
Kelly, S., Beaumont, C., Jamieson, R.A., 2022. Eohimalayan metamorphism and subsequent tectonic quiescence explained. Earth Planet. Sci. Lett. 584, 117350.
Klingelhoefer, F., Lafoy, Y., Collot, J., Cosquer, E., Geli, L., Nouze, H., Vially, R., 2007. Crustal structure of the basin and ridge system west of New Caledonia (southwest Pacific) from wide-angle and reflection seismic data. J. Geophys. Res., Solid Earth 112 (B11).
Kohn, M.J., 2014. Himalayan metamorphism and its tectonic implications. Annu. Rev. Earth Planet. Sci. 42, 381–419.
Lee, J., Hacker, B.R., Dinklage, W.S., Wang, Y., Gans, P., Calvert, A., McClelland, W., 2000. Evolution of the Kangmar Dome, southern Tibet: structural, petrologic, and thermochronologic constraints. Tectonics 19 (5), 872–895.
Li, Y.P., Robinson, A.C., Lapen, T.J., Righter, M., Stevens, M.K., 2020. Muztaghata Dome Miocene Eclogite facies metamorphism: a record of lower crustal evolution of the NE Pamir. Tectonics 39 (7), e2019TC005917.
Lihter, I., Larson, K.P., Smit, M.A., Cottle, J.M., Ashley, K.T., Shrestha, S., 2022. Decrypting the polymetamorphic record of the Himalaya. Geology 50 (5), 588–592.
Martin, A.J., 2017. A review of Himalayan stratigraphy, magmatism, and structure. Gondwana Res. 49, 42–80.
Martin, C.R., Jagoutz, O., Upadhyay, R., Royden, L.H., Eddy, M.P., Bailey, E., Weiss, B.P., 2020. Paleocene latitude of the Kohistan–Ladakh arc indicates multistage India–Eurasia collision. Proc. Natl. Acad. Sci. 117 (47), 29487–29494.
Maunder, B., Prytulak, J., Goes, S., Reagan, M., 2020. Rapid subduction initiation and magmatism in the Western Pacific driven by internal vertical forces. Nat. Commun. 11 (1), 1–8.
McCarthy, A., Chelle-Michou, C., Müntener, O., Arculus, R., Blundy, J., 2018. Subduction initiation without magmatism: the case of the missing Alpine magmatic arc. Geology 46 (12), 1059–1062.

Meng, J., Gilder, S.A., Li, Y., Wang, C., Liu, T., 2020. Expanse of Greater India in the late Cretaceous. Earth Planet. Sci. Lett. 542, 116330.
Molnar, P., Stock, J.M., 2009. Slowing of India's convergence with Eurasia since 20 Ma and its implications for Tibetan mantle dynamics. Tectonics 28 (3).
Murphy, M.A., 2007. Isotopic characteristics of the Gurla Mandhata metamorphic core complex: implications for the architecture of the Himalayan orogen. Geology 35 (11), 983–986.
Murphy, M.A., Yin, A., 2003. Structural evolution and sequence of thrusting in the Tethyan fold-thrust belt and Indus-Yalu suture zone, southwest Tibet. Geol. Soc. Am. Bull. 115 (1), 21–34.
Myrow, P.M., Hughes, N.C., Paulsen, T.S., Williams, I.S., Parcha, S.K., Thompson, K.R., Ahluwalia, A.D., 2003. Integrated tectonostratigraphic analysis of the Himalaya and implications for its tectonic reconstruction. Earth Planet. Sci. Lett. 212 (3–4), 433–441.
Pan, G., Ding, J., Yao, D., Wang, L., 2004. Geological Map of the Qinghai-Xizang (Tibet) Plateau and Adjacent Areas: Chengdu. Chengdu Cartographic Publishing House.
Powell, C.M., Roots, S.R., Veevers, J.J., 1988. Pre-breakup continental extension in East Gondwanaland and the early opening of the eastern Indian Ocean. Tectonophysics 155 (1–4), 261–283.
Qi, Y., Hawkesworth, C.J., Wang, Q., Wyman, D.A., Li, Z.X., Dong, H., Zhang, X.Z., 2021. Syn-collisional magmatic record of Indian steep subduction by 50 Ma. Geol. Soc. Am. Bull. 133 (5–6), 949–962.
Robinson, D.M., DeCelles, P.G., Patchett, P.J., Garzione, C.N., 2001. The kinematic evolution of the Nepalese Himalaya interpreted from Nd isotopes. Earth Planet. Sci. Lett. 192 (4), 507–521.
Robinson, D.M., DeCelles, P.G., Copeland, P., 2006. Tectonic evolution of the Himalayan thrust belt in western Nepal: implications for channel flow models. Geol. Soc. Am. Bull. 118 (7–8), 865–885.
Robinson, D.M., Martin, A.J., 2014. Reconstructing the Greater Indian margin: a balanced cross section in central Nepal focusing on the Lesser Himalayan duplex. Tectonics 33 (11), 2143–2168.
Robinson, D.M., Metcalf, K., 2020. Evaluating the evolution of the southern Himalayan-Tibetan orogeny: What happened during Paleocene-Eocene time?. NSF-EAR Award Abstract 2020444.
Robinson, D.M., Khanal, S., Olree, E., Bhattacharya, G., Mandal, S., 2021. Controls of stratigraphic architecture on along strike cooling age patterns. Terra Nova 33 (2), 129–136.
Smit, M.A., Hacker, B.R., Lee, J., 2014. Tibetan garnet records early Eocene initiation of thickening in the Himalaya. Geology 42 (7), 591–594.
Song, P., Din, L., Zhao, T., Li, J., Yue, Y., Xie, J., 2022. Paleomagnetism and geochronology of upper Eocene volcanic rocks from the western Qiangtang block: constraints on the post-collisional shortening in western Tibet. Glob. Planet. Change, 103953.
Stern, R.J., Gerya, T., 2018. Subduction initiation in nature and models: a review. Tectonophysics 746, 173–198.
Van Hinsbergen, D.J., Kapp, P., Dupont-Nivet, G., Lippert, P.C., DeCelles, P.G., Torsvik, T.H., 2011a. Restoration of Cenozoic deformation in Asia and the size of Greater India. Tectonics 30 (5).
Van Hinsbergen, D.J., Steinberger, B., Doubrovine, P.V., Gassmöller, R., 2011b. Acceleration and deceleration of India-Asia convergence since the Cretaceous: roles of mantle plumes and continental collision. J. Geophys. Res., Solid Earth 116 (B6).
Van Hinsbergen, D.J., Lippert, P.C., Dupont-Nivet, G., McQuarrie, N., Doubrovine, P.V., Spakman, W., Torsvik, T.H., 2012. Greater India Basin hypothesis and a two-stage Cenozoic collision between India and Asia. Proc. Natl. Acad. Sci. 109 (20), 7659–7664.
Wang, R., Collins, W.J., Weinberg, R.F., Li, J.X., Li, Q.Y., He, W.Y., Stern, R.A., 2016. Xenoliths in ultrapotassic volcanic rocks in the Lhasa block: direct evidence for crust–mantle mixing and metamorphism in the deep crust. Contrib. Mineral. Petrol. 171 (7), 1–19.
Webb, A.A.G., Yin, A., Harrison, T.M., Célérier, J., Burgess, W.P., 2007. The leading edge of the Greater Himalayan Crystalline complex revealed in the NW Indian Himalaya: implications for the evolution of the Himalayan orogen. Geology 35 (10), 955–958.
Webb, A.A.G., 2013. Preliminary balanced palinspastic reconstruction of Cenozoic deformation across the Himachal Himalaya (northwestern India). Geosphere 9 (3), 572–587.
Wu, F.Y., Liu, X.C., Liu, Z.C., Wang, R.C., Xie, L., Wang, J.M., He, S.X., 2020. Highly fractionated Himalayan leucogranites and associated rare-metal mineralization. Lithos 352, 105319.
Yi, Z., Wang, T., Meert, J.G., Zhao, Q., Liu, Y., 2021. An initial collision of India and Asia in the equatorial humid belt. Geophys. Res. Lett. 48 (9), e2021GL093408.
Yin, A., 2006. Cenozoic tectonic evolution of the Himalayan orogen as constrained by along-strike variation of structural geometry, exhumation history, and foreland sedimentation. Earth-Sci. Rev. 76 (1–2), 1–131.
Yin, A., Harrison, T.M., 2000. Geologic evolution of the Himalayan-Tibetan orogen. Annu. Rev. Earth Planet. Sci. 28 (1), 211–280.
Zhang, L.Y., Ducea, M.N., Ding, L., Pullen, A., Kapp, P., Hoffman, D., 2014. Southern Tibetan Oligocene–Miocene adakites: a record of Indian slab tearing. Lithos 210, 209–223.
Zou, H., 2014. Error Propagation. Treatise on Geochemistry 2nd Edition, vol. 15, pp. 33–42.